Astron. Astrophys. 345, 531–546 (1999)

ASTRONOMY AND ASTROPHYSICS

V606 Centauri: an early-type eclipsing contact binary⋆

Reinald Lorenz[1], **Pavel Mayer**[2], **and Horst Drechsel**[1]

[1] Dr. Remeis-Sternwarte Bamberg, Astronomisches Institut der Universität Erlangen-Nürnberg, Sternwartstrasse 7, D-96049 Bamberg, Germany
[2] Astronomical Institute, Charles University, V Holešovičkách 2, CZ-180 00 Praha 8, Czech Republic

Received 10 August 1998 / Accepted 9 December 1998

Abstract. We present a spectroscopic and photometric analysis of the early-type eclipsing binary V606 Cen. Based on new high-resolution CCD spectra the first radial velocity curve of this system is given, which allows for an accurate determination of radial velocity amplitudes ($K_1 = 181.8\,\mathrm{km\,s^{-1}}$, $K_2 = 345.2\,\mathrm{km\,s^{-1}}$) and the spectroscopic mass ratio $q_{\rm spec} = 0.527$. Moreover, equivalent widths are listed. The line strengths of He I 4922 show strong variations with the orbital phase, related to the so-called (and hitherto unexplained) "Struve-Sahade effect". In this context, some aspects concerning the determination of equivalent widths in close binary systems are discussed, with special reference to the influence of the ellipsoidal light variations. For the first time, photoelectric UBV light curves of V606 Cen are presented, which were solved with the MORO code, based on the Wilson-Devinney model. The first set of solutions was achieved with effective temperatures according to the previous spectral classification B1–2 Ib/IIb, but the derived absolute dimensions, surface gravities, as well as an investigation of the equivalent widths led to a revision of the spectral type. We now suggest B0–0.5 V for the primary, and B2–3 V for the secondary component, respectively. Using the corresponding effective temperatures, another light curve analysis was performed, yielding the following absolute dimensions: $M_1 = 14.7\,\mathrm{M}_\odot$, $M_2 = 8.0\,\mathrm{M}_\odot$, $R_1 = 6.8\,\mathrm{R}_\odot$, $R_2 = 5.2\,\mathrm{R}_\odot$, $\log L_1/\mathrm{L}_\odot = 4.48$, and $\log L_2/\mathrm{L}_\odot = 3.74$. In all cases, a contact configuration is found. The evolutionary state of V606 Cen is discussed in the light of modern evolutionary grids. It turns out that this contact system was formed during the slow phase of case A mass transfer after reversal of its mass ratio. In this respect it is similar to other early-type contact binaries such as V382 Cyg, V701 Sco or RZ Pyx.

Key words: stars: binaries: eclipsing – stars: binaries: spectroscopic – stars: early-type – stars: fundamental parameters – stars: individual: V 606 Cen

1. Introduction

The early-type eclipsing binary V606 Cen (HD 115937, SAO 252281, CD −59°4688, CPD −59°4923) was discovered by Swope (1939), and, independently, by Hertzsprung (1950). Hertzsprung classified the light curve as β Lyr type and gave the ephemeris:

$$Pri.\,Min. = \text{hel. JD}\,2427952.354 + 1\overset{\mathrm{d}}{.}495108 \cdot \mathrm{E}.$$

In the GCVS, the orbital period is listed as $1\overset{\mathrm{d}}{.}495093$, the spectral type as B1–2 Ib/II (taken from Houk & Cowley 1975), the magnitude at maximum V=9.4, and the depths of the minima as 0.85 and 0.4 mag. The binary is contained in the catalog "Southern Luminous Stars" (Stephenson & Sanduleak 1971) as No. 3043 with spectral type OB^-, and in Eggen's (1978) compilation of early-type contact binaries. This author gives photometric indices and a photometric spectral type B1 III. Since little more seems to be known about this system, a detailed investigation was performed in the frame of our program of photometric and spectroscopic analysis of early-type binaries. The first results of our measurements – three times of minima – were already published by Mayer et al. (1992).

Based on high-resolution CCD spectroscopy (Sect. 2.1) taken at ESO, La Silla, we are able to present the first radial velocity curve of V606 Cen (Sect. 2.2). Moreover, equivalent widths (EWs) have been determined. In order to obtain the true EWs, in close binary systems the observed EWs have to be corrected with respect to the actual and phase-dependent contribution of both stellar components to the composite continuum. Hence, also the ellipsoidal light variation must be taken into account, as discussed in Sect. 2.3. The EWs of He I 4922 show significant variations with the orbital phase. This so-called "Struve-Sahade effect" is briefly discussed in Sect. 2.3, too.

The first photoelectric UBV light curves of V606 Cen, which we obtained with the ESO 50cm-telescope, are presented in Sect. 3.1. The light curve analysis was caried out using the MORO code, which is based on the Wilson-Devinney model (see Sect. 3.2). We achieved two sets of solutions: one with effective stellar temperatures corresponding to the spectral classification of Houk & Cowley (1975) ("solution C"), the other with higher effective temperatures ("solution H"). Absolute dimensions have been calculated, and the problem concerning the effective temperatures is thoroughly discussed (Sect. 4.1). There are strong arguments in favour of light curve solution "H", which is preferred here. The evolutionary state of V606 Cen is studied in Sect. 4.2, and comparisons with stellar evolution grids are made there. Some conclusions are drawn in Sect. 5.

Send offprint requests to: R. Lorenz

⋆ Based on observations collected at the European Southern Observatory, La Silla, Chile

V606 Cen is one of the very few early-type contact binaries, for which accurate absolute dimensions can be determined, and it is therefore of special importance with respect to tests of modern stellar evolution concepts.

2. Spectroscopy

2.1. Observations and data reduction

Altogether 26 high resolution CCD spectra of V606 Cen were collected using the ESO 1.52m telescope equipped with the ECHELEC Echelle spectrograph and the ESO 1.4m CAT feeding the 3.6m coudé Echelle spectrograph CES. The observations with the ESO 1.52m telescope took place in February 1992 and 1993, when 9 spectra were taken. The average linear dispersion was 3.8 Å mm^{-1}, with a slit width in the range 1.4″ to 2.5″, equivalent to a resolving power of 23000 to 32000. With the RCA #13 CCD chip the useful wavelength interval was about 300 Å wide. Unfortunately, it turned out that with V606 Cen (V=$9\overset{\mathrm{m}}{.}4$ at maximum) we already reached the limits of ECHELEC. Despite exposure times up to more than two hours (depending on the weather conditions), it was nearly impossible to obtain spectra with satisfying signal-to-noise ratios, say, better than 50.

Hence, for further measurements we decided to use the ESO CAT/CES with its limiting magnitude considerably fainter than that of ECHELEC, and collected a total of 17 spectra with this instrument in April 1994. Exposure times from 45 to 75 minutes allowed for S/N ratios of about 80 to 120. As the spectral resolution of the CES, even with the Short Camera, is extremely high (up to about 56000 at a slit width of 2″), only one spectral line could be covered with the RCA #9 CCD chip. The linear dispersion was 2.6 Å mm^{-1} in the spectral region around Hβ and 3.6 Å mm^{-1} around Hα, the useful wavelength range being about 40 Å and 55 Å, respectively.

Immediately before or after each stellar spectrum, a Th-Ar comparison spectrum was taken, and in all nights, numerous lamp flatfields as well as bias frames were exposed. A journal of our V606 Cen spectrograms is given in Table 1.

The reduction was performed with the ESO MIDAS image processing package. A detailed description of the data reduction of the ECHELEC spectra was given by Lorenz et al. (1994). The CAT spectra of each night were divided by a mean flatfield frame, obtained by averaging all flatfields of the respective night. Moreover, an average bias frame was substracted. Especially the wavelength calibration was carried out with great care. Each CAT/CES star spectrum was wavelength calibrated with its corresponding Th-Ar arc spectrum, in order to obtain accurate individual dispersion relations.

2.2. The radial velocity curve

With the ESO CAT/CES the absorption lines He I 4922 and Hα were measured, whereas the ECHELEC spectra comprised wavelength regions around Hβ. We used 16 out of 17 CAT spectra for the radial velocity determination, while only three ECHELEC spectra were selected due to the reasons mentioned above. As their signal-to-noise ratios were about one third of those of the CAT spectra, the radial velocity data were weighted accordingly.

Apart from eclipse phases, the observed line features could clearly be resolved into the profiles of the primary and secondary stellar component. Hence, the lines were fitted with two Gaussian profiles using the Newton-Raphson method for optimizing the central wavelengths, full-widths at half maximum (FWHMs) and absorption amplitudes. Since the secondary minimum is an occultation (see Sect. 3.1), the spectrum during the totality is identical with the one of the primary stellar component. Hence, the CAT spectrum taken at phase 0.534 (a little outside of totality, but with the secondary's contribution to the composed light being only about 5%) could be used for the determination of radial velocity and equivalent width, too. In this case, the fit was performed with one single Gaussian only.

Radial velocities were then calculated including the barycentric correction, and the orbital phases were determined with the ephemeris

Table 1. Journal of spectra

hel. JD[a] −2 440 000	ϕ[b]	t (s)[c]	spectral range (Å) or obs. line	instr.[d]
8676.7192	0.587	7200	4590–4905	ECH
8677.7318	0.264	7080	4590–4905	ECH
9023.7818	0.720	2773	4630–4950	ECH
9024.7159	0.345	5400	4630–4950	ECH
9025.8528	0.105	5400	4630–4950	ECH
9026.7862	0.730	5400	4630–4950	ECH
9026.8626	0.781	6600	4630–4950	ECH
9027.6967	0.339	8100	4630–4950	ECH
9029.8218	0.760	6600	4630–4950	ECH
9448.6061	0.865	3600	He I 4922	CAT
9448.6964	0.925	3600	He I 4922	CAT
9449.6069	0.534	3600	He I 4922	CAT
9449.7221	0.611	3600	He I 4922	CAT
9449.7652	0.640	3600	He I 4922	CAT
9449.8714	0.711	3600	He I 4922	CAT
9450.6166	0.209	3600	He I 4922	CAT
9450.6659	0.242	4200	He I 4922	CAT
9450.7159	0.276	4200	He I 4922	CAT
9450.7729	0.314	4500	He I 4922	CAT
9451.6041	0.870	3600	He I 4922	CAT
9452.6702	0.583	2700	H α	CAT
9452.7778	0.655	3600	H α	CAT
9452.8681	0.715	3600	H α	CAT
9452.9118	0.745	3600	H α	CAT
9453.6431	0.234	3600	He I 4922	CAT
9453.6869	0.263	3600	He I 4922	CAT

[a] time of mid-exposure
[b] orbital phase according to:
hel. JD $2448687\overset{\mathrm{d}}{.}8026 + 1\overset{\mathrm{d}}{.}4950996 \cdot \mathrm{E}$ (see Sect. 3.1)
[c] exposure time
[d] instrument used for observation: ECH=1.52m ESO telescope + ECHELEC; CAT=1.4m ESO CAT/CES

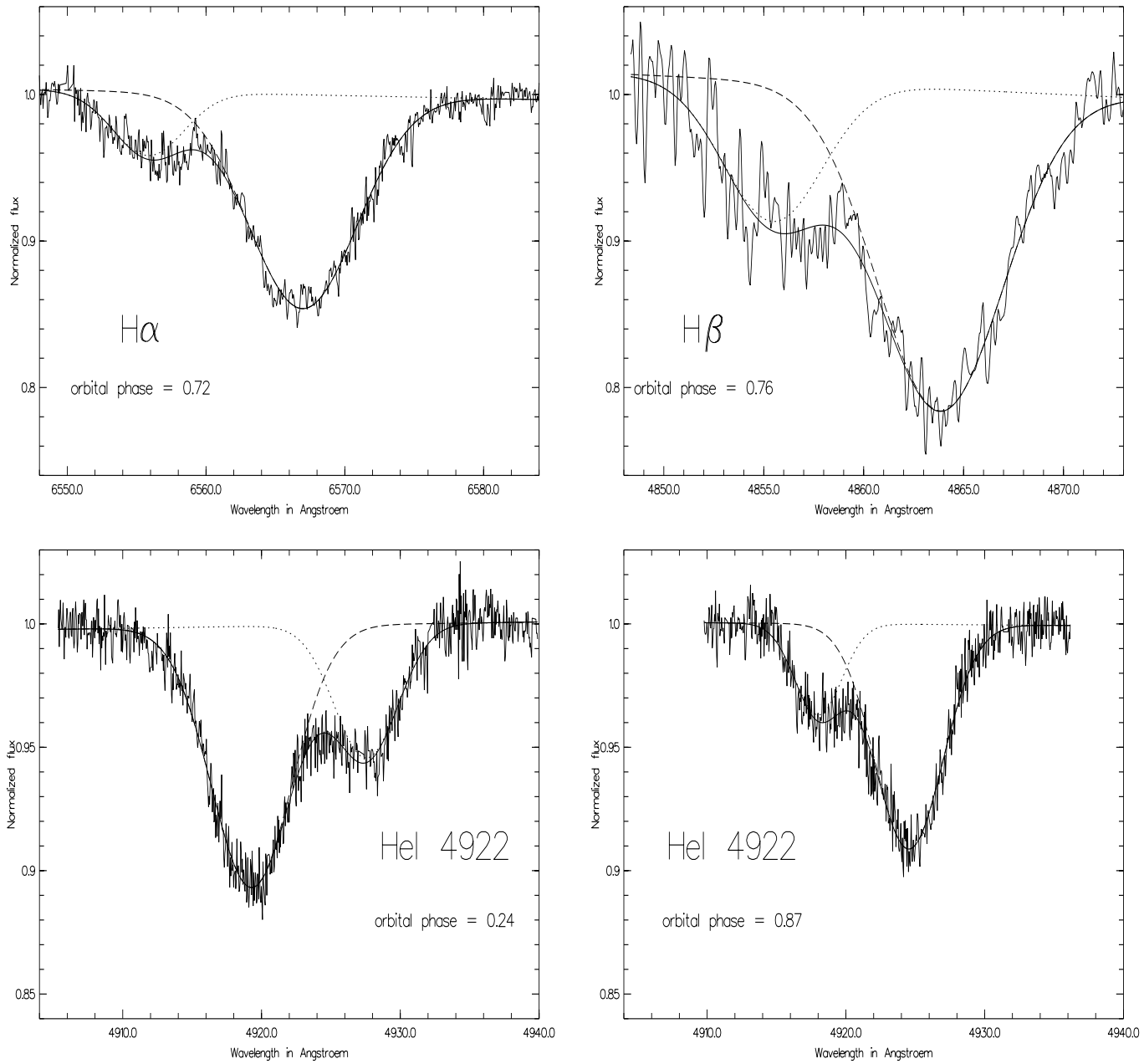

Fig. 1. Typical line features of Hα, Hβ, and He I 4922; fitted Gaussian profiles for the primary and secondary component are drawn as dashed and dotted lines, respectively, the resulting fit curve is shown as solid line. The variation of the strength of the He I 4922 lines with the orbital phase is clearly visible. The Hβ spectrum was obtained with ECHELEC, all other spectra with CAT/CES.

$$Pri.\,Min. = \text{hel. JD}2448687.8026 + 1\overset{\text{d}}{.}4950996 \cdot \text{E},$$

assuming a circular orbit (cf. Sect. 3.1). Typical observed features of the Hα, Hβ, and He I 4922 lines are presented in Fig. 1, which also shows the fitted Gaussian profiles.

The radial velocities of each stellar component determined this way were fitted with sine functions, with the amplitudes A_i and systemic velocities γ_i as free parameters. For the primary (index "1") and secondary (index "2") the following values were achieved:

$$A_1 = -180.1\text{km s}^{-1}, \quad \gamma_1 = 23.6\text{km s}^{-1} \qquad \text{and}$$

$$A_2 = \quad 343.4\text{km s}^{-1}, \quad \gamma_2 = \quad 3.0\text{km s}^{-1} \quad ,$$

respectively.

The large difference of the systemic velocities, which of course cannot be real, is a well-known and so far unexplained effect in early-type SB2 systems and was already discussed by Mayer et al. (1991). In order to obtain consistent radial velocity curves for both stellar components, the arithmetic mean of γ_1 and γ_2 was taken as the systemic velocity of V606 Cen:

$$\gamma_0 = 14.3\text{km s}^{-1} \pm 2.5\text{km s}^{-1} \quad .$$

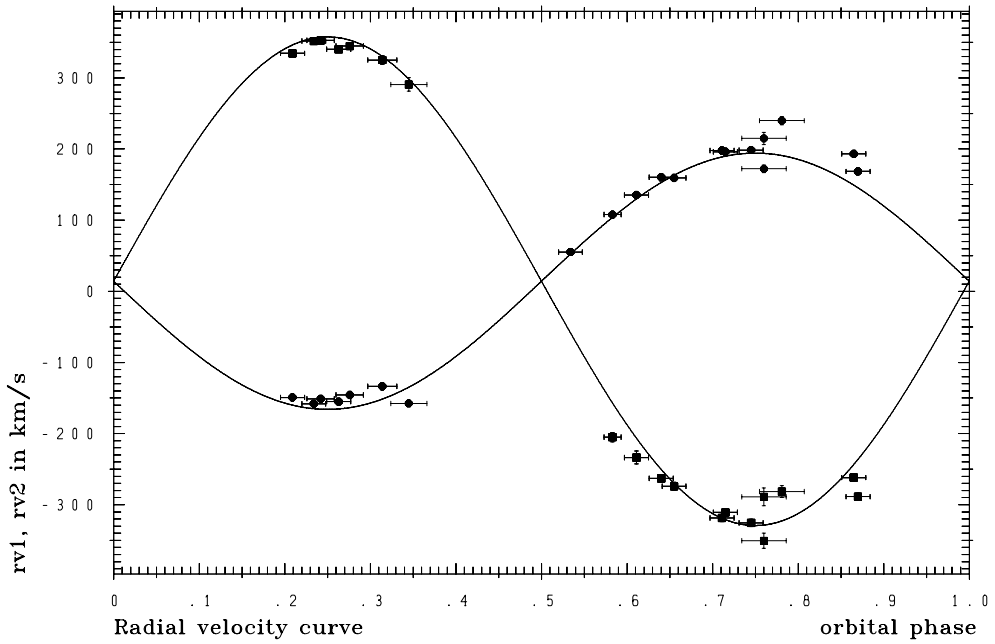

Fig. 2. Radial velocities of the primary (filled circles) and the secondary (filled squares). The computed radial velocity curves are also shown.

Table 2. Individual radial velocity measurements of the spectral lines Hα, Hβ and He I 4922

line	hel. JD-2440000	ϕ^a	v_1 (km s^{-1})	$(\delta v_1)_{\rm fit}{}^b$	v_2 (km s^{-1})	$(\delta v_2)_{\rm fit}{}^b$
Hα	9452.670	0.583	107.9	2.8	−205.0	6.6
	9452.778	0.655	159.3	2.0	−274.2	5.6
	9452.868	0.715	196.2	1.6	−310.8	4.4
	9452.912	0.745	198.5	1.7	−325.5	5.2
Hβ	9029.822	0.760	172.3	5.2	−350.7	10.8
He I 4922	9024.716	0.345	−157.6	4.6	290.7	9.5
	9026.863	0.781	239.9	5.9	−281.4	8.5
	9029.822	0.762	214.9	8.6	−288.8	12.4
	9448.606	0.865	193.2	2.1	−261.8	5.4
	9449.607	0.534	55.2	1.7	$-^c$	$-^c$
	9449.722	0.611	135.5	3.3	−233.7	9.1
	9449.765	0.640	160.4	2.0	−263.0	5.2
	9449.871	0.711	198.0	1.9	−318.5	5.1
	9450.617	0.209	−149.1	2.1	334.5	4.3
	9450.666	0.242	−151.0	1.9	352.7	3.9
	9450.716	0.276	−145.6	2.0	344.7	3.9
	9450.773	0.314	−133.5	2.7	325.1	5.8
	9451.604	0.870	168.5	2.2	−288.6	5.0
	9453.643	0.234	−158.0	1.8	351.8	4.0
	9453.687	0.263	−155.1	1.9	340.1	4.0

[a] orbital phase according to hel. JD $2448687^{\rm d}.8026 + 1^{\rm d}.4950996 \cdot {\rm E}$ (see Sect. 3.1)
[b] mean fit error in km s^{-1} (χ^2-based estimation of profile fit quality)
[c] due to total eclipse only primary line visible

The given error is due to the uncertainty of the $\gamma_{1,2}$ values, whereas the real error is of course larger, and might amount to about $|\gamma_1 - \gamma_2|$.

The radial velocities were now fitted again with sine functions

$$\gamma_0 + K_i \sin\phi \quad ,$$

with γ_0 as fixed parameter and the radial velocity amplitudes K$_i$ ($i = 1, 2$) as adjustable quantities; ϕ denotes the orbital phase. The result was:

$$K_1 = -181.8\text{km s}^{-1} \pm 2.9\text{km s}^{-1}$$
$$K_2 = \quad 345.2\text{km s}^{-1} \pm 3.7\text{km s}^{-1} \quad ,$$

and the spectroscopic mass ratio of V606 Cen therefore is

$q_{\rm spec} = K_1/K_2 = M_2/M_1 = 0.527 \pm 0.017.$

Note that the radial velocity amplitudes (A_1, K_1 and A_2, K_2) are rather insensitive with respect to the obtained values γ_1, γ_2, γ_0 of the systemic velocities. Hence, the determination of γ_0 as the mean of γ_1 and γ_2 is an acceptable procedure. The given errors are formal fit errors.

This procedure to derive accurate radial velocities from spectra consisting of blended line features has already proven its reliability in the case of the multiple system SZ Cam (Lorenz et al., 1998), showing still stronger blended profiles than those of V606 Cen are. In order to exclude eventual systematic fit errors, checks with synthetic spectra had been carried out, which yielded an accuracy of about 3 km s^{-1}. The results had also been confirmed by radial velocities derived by use of the KOREL code (Hadrava, 1995, Drechsel et al., 1997), which is a Fourier transform method for disentangling composite stellar spectra of binary or multiple stars. In the case of V606 Cen, KOREL was applied on the He I 4922 lines, yielding radial velocity amplitudes K_1 = -185.5 km s^{-1}, K_2 = 347.2 km s^{-1}, and the spectroscopic mass ratio $q_{\rm KOREL} = 0.531$, which nearly perfectly fit the results of the radial velocity analysis described above.

The differences between calculated (i.e. fitted) and observed radial velocities of Hα are very similar to those of He I 4922 in the respective range of the orbital phase, and no systematic deviation is present. Only the Hβ based velocities from one ECHELEC spectrum (given one third weight of the CAT spectra) are about 25 km s^{-1} below the fitted curve both for the primary and secondary component.

The individual radial velocities and corresponding χ^2-based estimations of the profile fit quality are listed in Table 2, the radial velocity curves of the primary and secondary component as well as the computed sine functions are shown in Fig. 2.

2.3. Determination of equivalent widths

In close binary systems, the measured equivalent widths $EW_{\rm obs}$ always refer to the composite continuum of both stellar components (and, additionally, to that of an eventual third body). In order to find out the true equivalent widths EW, the fraction of light originating from each component must be known. This is the case, if a unique light curve solution exists, and therefore the effective temperatures, the surface potentials and radii of the stars involved are defined. Obviously, due to their distortion and eventual eclipses, the flux descending from each star in direction to the observer varies with the orbital phase. This variable total flux apart from eclipses in the light curves of close binary systems is called the "ellipsoidal light variation".

Using the stellar parameters derived from the light curve solution the fluxes originating from all surface elements of both stars can be computed by means of Planck functions, taking into account the limb darkening, gravitational darkening and the reflexion effect. Then the incoming light $l_{\rm i}(\phi,\lambda)$, (i=1,2 denotes the primary and secondary, respectively) is the sum over the fluxes emitted in the observer's direction of all surface elements facing the observer (taking the distortion of the stellar surfaces and eclipses into consideration). The fractional flux of each component can then be described as:

$$F_{\rm c,i}(\lambda,\phi) = \frac{l_{\rm i}(\lambda,\phi)}{l_1(\lambda,\phi)+l_2(\lambda,\phi)+l_3(\lambda)} \quad , \qquad (1)$$

with $l_3(\lambda)$ being the phase independent contribution of a third body to the total light.

It might be of general interest to show by means of Eq. 1, how the stellar components of close binaries with different system configurations contribute to this effect. For this purpose, the solutions of V light curves of the detached system SZ Cam (O9V + B0.5V; cf. Lorenz et al. 1998), the semi-detached system AB Cru (O8 + B0.5; cf. Lorenz et al. 1994) and the contact binary V606 Cen are considered. On the left half of Fig. 3, the $F_{\rm c,i}(\lambda,\phi)$ values, i.e. the fractions of the total flux at 5550 Å as a function of the orbital phase are shown for the primary and secondary components of these binaries. In the case of SZ Cam, an additional third body contributes between 30 and 40% to the total light (crosses). Note, that the secondary minimum of V606 Cen is a total eclipse, so that at this point the primary provides the entire flux of this binary. The secondary minimum of AB Cru is also very nearly a total eclipse.

In order to demonstrate the ellipsoidal light variations in a different way, the right side of Fig. 3 shows the fraction of the maximum flux $l_{\rm i}(5550\,\text{Å},\phi)/l_{\rm i}(5550\,\text{Å},\phi=0.25)$ of each stellar component, with the primary and secondary flux being normalized to 1.0 at orbital phase 0.25, respectively. Apart from eclipse phases, the slightly distorted stars in the detached system SZ Cam show only moderate light variations of less than 10%. The AB Cru secondary, which fills its critical Roche-lobe, undergoes a considerable loss of brightness of about 20% between orbital phases 0.75 and 1.00 (or 0.25 and 0.00), whereas the flux descending from the nearly spherical primary component is almost constant. Due to its contact configuration, the secondary of V606 Cen behaves quite similar as the AB Cru secondary, but the primary exhibits a strong ellipsoidal light variation of over 10%, too.

Following Eq. 1, the true equivalent widths with respect to the individual continua of the stellar components can be described as:

$$\begin{aligned} EW_{\rm i} &= EW_{\rm i,obs} \cdot F_{\rm c,i}^{-1}(\lambda,\phi) \\ &= EW_{\rm i,obs} \cdot \frac{l_1(\lambda,\phi)+l_2(\lambda,\phi)+l_3(\lambda)}{l_{\rm i}(\lambda,\phi)} \quad . \end{aligned} \qquad (2)$$

In practice $F_{\rm c}$ can be determined for the filter wavelength(s) of the analyzed light curve(s), for which the light curve program computes the individual fluxes $l_{\rm i}(\lambda,\phi)$. As the wavelengths of the spectral lines are different from these photometric filter wavelengths, Eq. 2 is only an approximation when determining true equivalent widths.

In case of V606 Cen, the observed lines were Hα, Hβ and He I 4922, whereas the filter wavelengths are λ=3500 Å, 4350 Å and 5550 Å , for U, B, and V, respectively. Using Planck functions $B_\lambda(T)$ the phase independent contribution of both

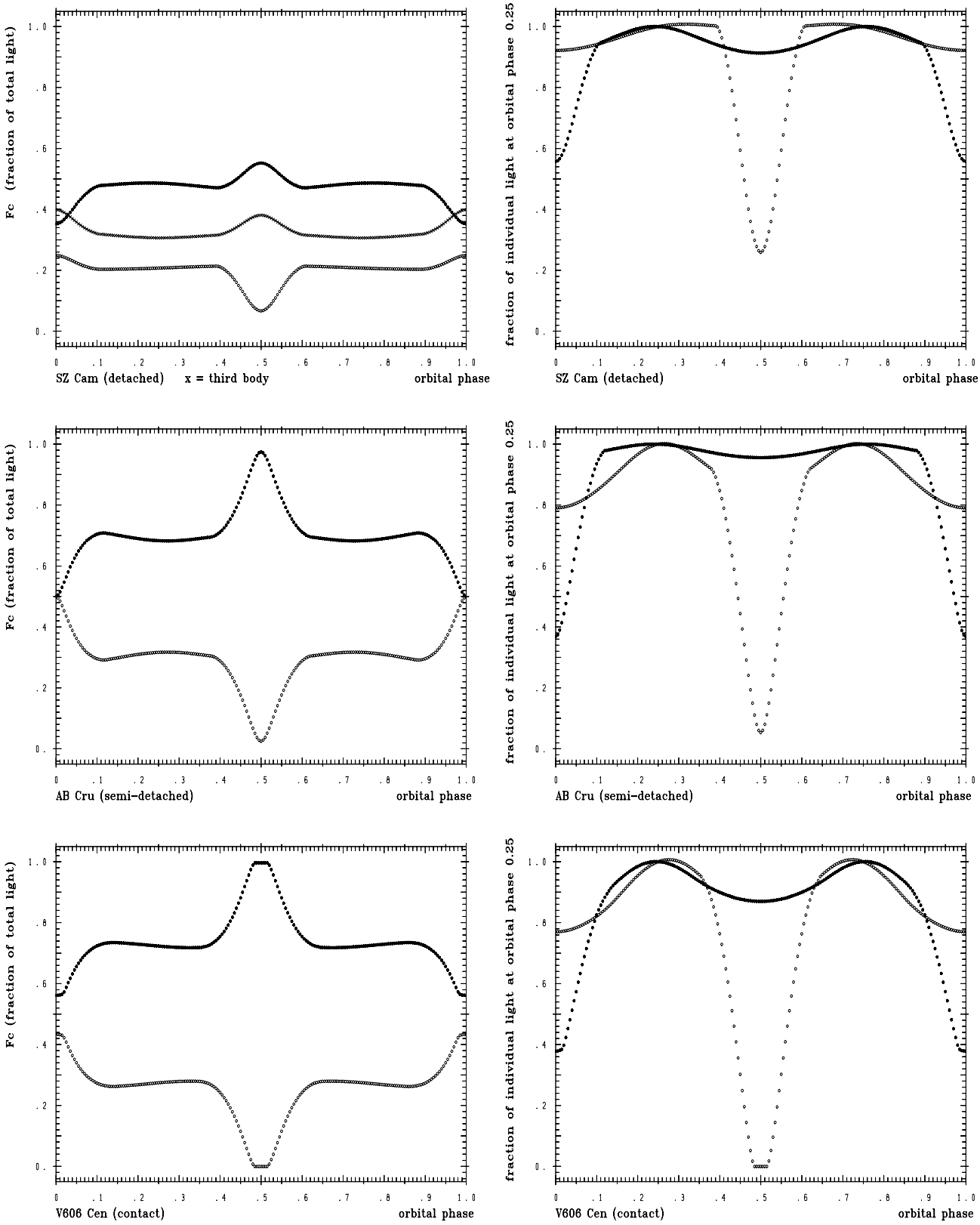

Fig. 3. Relative contribution of the stellar components of three early-type close binary systems with different system configurations to their composite spectral continua (left side), and fraction of the individual light of each component normalized to 1.0 at orbital phase 0.25 (right side). The data are based on V light curve solutions (see Lorenz et al. 1998 for SZ Cam, Lorenz et al. 1994 for AB Cru, and this paper, "H" solution, for V606 Cen). Filled circles denote primary, open circles secondary components. Note that in case of SZ Cam a third body (crosses) contributes about 30–40% to the total light. For details see text.

Table 3. Equivalent widths of Hα, Hβ, and He I 4922

line	ϕ^a	Instr.[b]	EW$_{obs}$[c] in Å		solution C				solution H			
					F_c[d]		EW[e] in Å		F_c[d]		EW[e] in Å	
			prim.	sec.	prim.	sec.	prim.	sec.	prim.	sec.	prim.	sec.
H α	0.583	CAT	1.76	0.30	0.781	0.218	2.25	1.38	0.786	0.212	2.24	1.42
H α	0.655	CAT	1.53	0.25	0.719	0.280	2.13	0.89	0.718	0.280	2.13	0.89
H α	0.715	CAT	1.44	0.28	0.722	0.277	1.99	1.00	0.720	0.278	2.00	1.01
H α	0.745	CAT	1.41	0.27	0.725	0.273	1.95	1.00	0.723	0.275	1.95	0.98
H β	0.760	ECH	1.69	0.51	0.727	0.271	2.33	1.88	0.724	0.273	2.33	1.87
He I 4922	0.209	CAT	0.75	0.31	0.731	0.267	1.03	1.16	0.728	0.269	1.03	1.15
He I 4922	0.234	CAT	0.60	0.24	0.728	0.270	0.82	0.88	0.725	0.273	0.83	0.88
He I 4922	0.242	CAT	0.77	0.31	0.727	0.271	1.06	1.15	0.724	0.274	1.06	1.13
He I 4922	0.263	CAT	0.71	0.30	0.724	0.274	0.98	1.08	0.722	0.276	0.98	1.09
He I 4922	0.276	CAT	0.62	0.32	0.723	0.276	0.86	1.15	0.721	0.277	0.86	1.16
He I 4922	0.314	CAT	0.63	0.35	0.719	0.279	0.88	1.24	0.718	0.280	0.88	1.25
He I 4922	0.345	ECH	0.49	0.12	0.719	0.280	0.68	0.43	0.718	0.279	0.68	0.43
He I 4922	0.534	CAT	0.84	-[f]	0.940	0.057	0.89	-[f]	0.942	0.055	0.89	-[f]
He I 4922	0.611	CAT	0.63	0.15	0.740	0.258	0.85	0.59	0.740	0.258	0.85	0.58
He I 4922	0.640	CAT	0.62	0.18	0.720	0.278	0.85	0.64	0.721	0.277	0.86	0.65
He I 4922	0.711	CAT	0.52	0.11	0.721	0.277	0.72	0.40	0.719	0.278	0.72	0.40
He I 4922	0.760	ECH	0.68	0.25	0.727	0.271	0.94	0.92	0.724	0.273	0.94	0.92
He I 4922	0.781	ECH	0.54	0.18	0.730	0.268	0.74	0.66	0.727	0.271	0.74	0.66
He I 4922	0.865	CAT	0.37	0.09	0.738	0.260	0.50	0.34	0.735	0.263	0.50	0.34
He I 4922	0.870	CAT	0.56	0.16	0.738	0.260	0.76	0.60	0.734	0.263	0.76	0.61
He I 4922	0.925	CAT	0.43	0.10	0.704	0.294	0.60	0.35	0.700	0.297	0.61	0.34

[a] orbital phase according to: hel. JD $2448687^{\rm d}.8026 + 1^{\rm d}.4950996 \cdot {\rm E}$
[b] spectrograph used for observation: ECH=ECHELEC, CAT=CAT/CES
[c] measured equivalent widths with respect to the composite continuum
[d] according to Eq. 1; see text
[e] true equivalent widths according to Eq. 2; see text
[f] due to total eclipse only primary line visible

stellar components to the total continuum for the different line wavelengths can be approximated:

$$F_{\rm p,i}(\lambda, T) = \frac{B_\lambda(T_{\rm i}) \cdot S_{\rm i}}{B_\lambda(T_1) \cdot S_1 + B_\lambda(T_2) \cdot S_2}$$

where $S_{\rm i}$ are the surfaces of the stellar components, and no third-light contribution is assumed. For V606 Cen ($l_3({\rm V}) << 1\%$) $F_{\rm p,i}(\lambda, T)$ amounts to:

$$\begin{aligned} F_{\rm p,1}(4861\,{\rm Å}, 19650\,{\rm K}) &= 0.745\,, \\ F_{\rm p,1}(4922\,{\rm Å}, 19650\,{\rm K}) &= 0.745\,, \quad \text{and} \\ F_{\rm p,1}(6562\,{\rm Å}, 19650\,{\rm K}) &= 0.730 \end{aligned}$$

for the primary, and to

$$\begin{aligned} F_{\rm p,2}(4861\,{\rm Å}, 15400\,{\rm K}) &= 0.255\,, \\ F_{\rm p,2}(4922\,{\rm Å}, 15400\,{\rm K}) &= 0.255\,, \quad \text{and} \\ F_{\rm p,2}(6562\,{\rm Å}, 15400\,{\rm K}) &= 0.270 \end{aligned}$$

for the secondary component.

As discussed later (see Sects. 3.2, 4.1) we give light curve solutions for two sets of effective temperatures T_1 and T_2 for the primary and secondary component (solution "C": $T_1 = 19650\,{\rm K}, T_2 = 15400\,{\rm K}$, and solution "H": $T_1 = 29200\,{\rm K}, T_2 = 21770\,{\rm K}$), respectively, both yielding slightly different luminosity ratios.

The $F_{\rm c}$ factors at 5550 Å (V colour) at orbital phase 0.25 are: $F_{\rm c,1}(V, 0.25) = 0.726$ and $F_{\rm c,2}(V, 0.25) = 0.272$ for solution C, and $F_{\rm c,1}(V, 0.25) = 0.723$ and $F_{\rm c,2}(V, 0.25) = 0.275$ for solution H, respectively. The third light contribution in both cases amounts to 0.002 (see Table 8).

To check whether the $F_{\rm c}$ factors for the V curve can be used for the determination of true equivalent widths of the three spectral lines mentioned, they have to be compared with the $F_{\rm p}$ values given above. The deviations are about 3% (Hβ, He I 4922) and 0.5% (Hα) for the primary, and about 6% (Hβ, He I 4922) and 0.1% (Hα) for the secondary component, respectively. Therefore, it is acceptable to use Eq. 2 for the determination of the true equivalent widths. The corresponding results together with the measured equivalent widths and the fractions of total light for both components as a function of the orbital phase are listed in Table 3. It is evident that the true equivalent widths belonging to both light curve solutions are nearly identical. The true equivalent width of the He I 4922 line as a

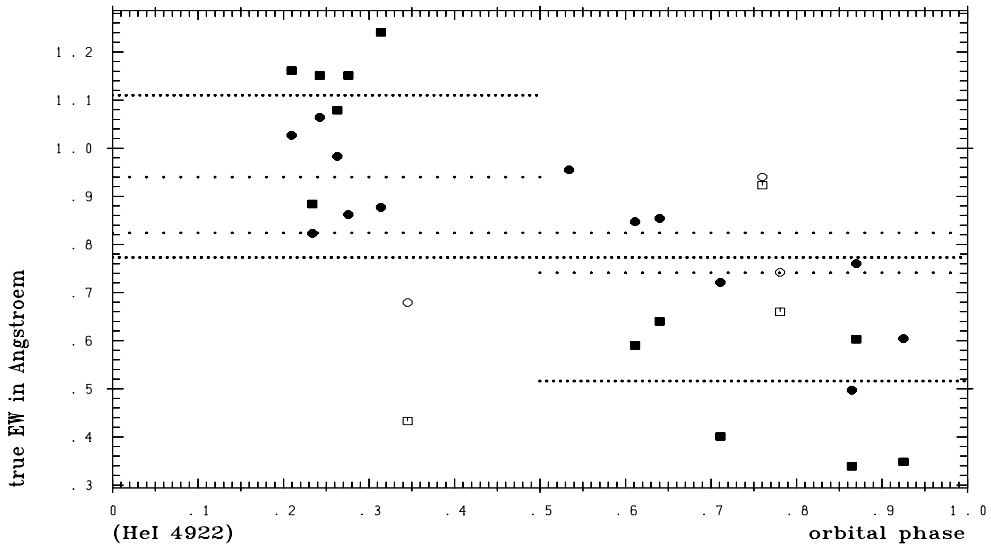

Fig. 4. True equivalent widths of He I 4922 as a function of orbital phase, corresponding to the "H" light curve solution. Circles denote the primary, squares the secondary component, respectively. Filled symbols refer to data based on CAT, open symbols to those based on ECHELEC spectra. Overall mean values of all primary and secondary equivalent widths are indicated as wide and narrow dotted lines across the full width of the figure. Those referring to CAT measurements in the phase ranges $0 < \phi \leq 0.5$ and $0.5 < \phi \leq 1.0$ are indicated as lines spreading over the corresponding phase intervals only.

function of orbital phase for solution H is shown in Fig. 4. Circles refer to the primary, squares to the secondary component, filled symbols to equivalent widths derived from CAT spectra, open symbols to those derived from ECHELEC spectra. Mean values of all data for the primary as well as for the secondary, which amount to 0.82 Å and 0.77 Å, are indicated as wide and condensed dotted lines, respectively.

Looking at the CAT measurements, which have been obtained in 6 consecutive nights, two groups of data points are present: all equivalent widths at phases $0 < \phi \leq 0.5$ (mean values = 0.94 Å and 1.11 Å for the primary and secondary, respectively) are significantly higher, whereas the very most of those at phases $0.5 < \phi \leq 1.0$ are considerably lower (mean values = 0.74 Å and 0.52 Å) than the overall mean values given above. This effect can be recognized for both stellar components, though it is stronger in case of the secondary.

Hence, the spectrum of the secondary appears to be considerably stronger when receding from the observer than during approach, and the primary shows an inverse behaviour. The phenomenon that optical stellar spectra exhibit variable strength, has been detected in massive binaries as well as in W-UMa systems. Recently, Stickland (1997) reported comparable effects in the UV spectra of the early-type binaries AO Cas, HD 47129 ("Plaskett's Star") and 29 CMa, calling them the "Struve-Sahade effect". Mostly the secondary spectrum appears stronger when the star is approaching the observer, but, similar to V606 Cen, another early-type contact binary, TU Mus (O8.5V), shows the inverse behaviour (Stickland et al. 1995). So far, no entirely satisfying explanation exists for it. Struve (1950) proposed that gaseous streams surrounding the stars were responsible for this phenomenon, whereas Gies et al. (1997) suggest heating of the stellar surfaces due to the proximity of the bow-shock region between the colliding winds of both stars. However, it seems that no explanation is yet completely satisfactory.

Our ECHELEC data show an inverse tendency compared with the CAT spectra, which were taken a few hundreds of epochs later, so that long-time variations of the equivalent widths could be suspected. On the other hand, the signal-to-noise ratios of the ECHELEC spectra compared with those taken with the CAT are poor, and the measurements in the phase range <0.5 are based on 1 spectrum, those of >0.5 on two spectra, only. Therefore, such long-term variations cannot be definitively proven here and must be checked by means of further observations.

3. Photometry

3.1. Observations

UBV photometry of V606 Cen was obtained with the ESO 0.5m telescope and its single channel photometer at La Silla, Chile, in four seasons: February 1992, January/February 1993, June 1993 and April 1994. An uncooled EMI 9789 QB tube served as photomultiplier, and a diaphragm of 21″ was used. Each integration lasted 1 second, and 20 to 30 integrations were averaged to form one raw data point. Informations about the comparison and check stars are given in Table 4. The data were transformed into the UBV system (the reduction process will be described in detail in a forthcoming paper by Mayer et al. 1999).

Altogether 929 measurements in each colour were used to form the UBV light curves with nearly complete phase coverage (see Fig. 5). A total of 7 eclipse minima was observed, three of them having already been discussed by Mayer et al. (1992). All minimum times are collected in Table 5. The minimum times of 1992 were recalculated and differ now by $0\overset{\mathrm{d}}{.}0003$ to $0\overset{\mathrm{d}}{.}0014$ from the values given in the previous paper.

Using all minimum times, the following new period and ephemeris can be calculated for V606 Cen:

$$Pri.Min. = \text{hel. JD}\,2448687.8026 + 1\overset{\mathrm{d}}{.}4950996 \cdot \mathrm{E}\ .$$
$$\pm 3 \qquad\qquad \pm 11$$

The period before the year 1992 appears to be slightly shorter ($1\overset{\mathrm{d}}{.}4950932$). The secondary eclipse minium of the light curve shows a phase of totality lasting about 0.030 in phase (about 1 hour). In order to facilitate the light curve analysis,

Table 4. UBV magnitudes for the measured stars

Star	HD	V	B-V	U-B
V606 Cen: maximum	115937	9.387	0.241	−0.648
pri. min.		10.167	0.252	−0.603
sec. min.		9.887	0.231	−0.669
comparison star	116003	6.907	0.008	−0.860
check star	115223	8.648	0.562	0.355

Table 5. The measured times of minima

hel. JD −2440000	m.e.	Epoch	O-C
8684.8131	0.0004	−2.0	+0.0007
8687.8023	0.0003	0.0	−0.0003
8690.7930	0.0003	2.0	+0.0002
9016.7240	0.0003	220.0	−0.0005
9019.7142	0.0004	222.0	−0.0005
9153.5261	0.0003	311.5	0.0000
9457.7794	0.0002	515.0	+0.0005

58 normal points in each colour were formed from the reduced observations, each one consisting of 11 to 22 individual measurements. Orbital phases were calculated using the ephemeris given above. The normal points together with colour indices are presented in Table 6.

The colour indices of the primary component (equal to the indices observed during secondary minimum) correspond to the spectral type B0.5 V, with interstellar reddening E(B-V)=0.51 mag.

3.2. Solution of the light curves

Using the normal points given in Table 6, the light curve analysis was performed with the MORO code, which is based on the Wilson-Devinney approach and additionally accounts for radiation pressure effects in detached or semi-detached close binary systems (for details see Drechsel et al. 1994a). Due to reasons discussed below, in the case of V606 Cen, the radiation pressure option was not used. The program was exclusively run in mode 2, which does not imply any restrictions with respect to the system configuration, and which connects the luminosity L_2 of the secondary component to its effective temperature T_2 by means of the Planck function. As for the light curve analysis only the ratio $(T_1/T_2)^4$ of the stellar components' temperatures is relevant, the primary temperature T_1 was fixed, and T_2 was adjusted. First, light curve solutions with $T_1 = 19650\,\mathrm{K}$, corresponding to the spectral type B1–2 Ib/II (according to Houk & Cowley, 1975) were achieved, later indicated as "solution C" (C for "cool"). As it will be shown in Sect. 4.1, there are good reasons to assume that the V606 Cen stellar components have higher effective temperatures than predicted by the previously given spectral type and the "C" solution indicates. Therefore, in a second step, the light curves were re-analyzed with $T_1 = 29200\,\mathrm{K}$

Table 6. Normal points of V606 Cen

No.	ϕ^a	U	B	V	B-V	U-B	Number of measurements
1	0.00491	3.7570	3.5043	3.2574	0.2469	0.2527	15
2	0.01044	3.7585	3.4992	3.2537	0.2456	0.2592	16
3	0.01765	3.7369	3.4830	3.2368	0.2462	0.2539	17
4	0.02506	3.6772	3.4239	3.1808	0.2432	0.2533	17
5	0.03362	3.5966	3.3468	3.1081	0.2387	0.2499	17
6	0.03913	3.5479	3.2984	3.0642	0.2342	0.2495	22
7	0.04691	3.4736	3.2340	2.9934	0.2406	0.2396	18
8	0.05502	3.4096	3.1726	2.9354	0.2372	0.2369	18
9	0.06374	3.3431	3.1073	2.8716	0.2357	0.2358	18
10	0.07382	3.2771	3.0462	2.8097	0.2364	0.2309	19
11	0.08422	3.2213	2.9894	2.7550	0.2344	0.2318	18
12	0.09598	3.1679	2.9374	2.7006	0.2368	0.2305	18
13	0.14098	3.0403	2.8162	2.5878	0.2284	0.2241	13
14	0.15922	3.0021	2.7839	2.5497	0.2341	0.2182	14
15	0.18004	2.9735	2.7561	2.5219	0.2341	0.2175	17
16	0.20362	2.9507	2.7324	2.4979	0.2345	0.2183	15
17	0.22480	2.9286	2.7173	2.4827	0.2345	0.2113	15
18	0.23541	2.9277	2.7083	2.4771	0.2312	0.2194	16
19	0.25949	2.9219	2.7088	2.4741	0.2347	0.2131	16
20	0.27311	2.9253	2.7123	2.4788	0.2334	0.2131	18
21	0.29203	2.9328	2.7195	2.4866	0.2328	0.2133	19
22	0.30825	2.9513	2.7394	2.5062	0.2332	0.2118	16
23	0.32978	2.9731	2.7616	2.5224	0.2393	0.2115	17
24	0.34279	2.9787	2.7693	2.5339	0.2354	0.2093	18
25	0.35211	2.9933	2.7819	2.5465	0.2354	0.2114	18
26	0.36847	3.0170	2.8064	2.5721	0.2342	0.2106	20
27	0.38982	3.0630	2.8519	2.6182	0.2338	0.2111	20
28	0.40787	3.1113	2.9010	2.6674	0.2335	0.2104	21
29	0.42592	3.1772	2.9691	2.7354	0.2337	0.2082	20
30	0.47916	3.3782	3.1893	2.9627	0.2265	0.1889	11
31	0.49764	3.3940	3.2052	2.9796	0.2255	0.1888	11
32	0.51087	3.3907	3.1962	2.9772	0.2190	0.1946	12
33	0.53200	3.3430	3.1472	2.9164	0.2308	0.1958	11
34	0.57276	3.1680	2.9599	2.7278	0.2321	0.2081	11
35	0.59593	3.0884	2.8795	2.6495	0.2300	0.2089	11
36	0.62852	3.0163	2.8051	2.5688	0.2362	0.2112	12
37	0.64788	2.9845	2.7746	2.5367	0.2379	0.2099	14
38	0.66610	2.9643	2.7577	2.5182	0.2395	0.2066	15
39	0.68808	2.9454	2.7333	2.4962	0.2371	0.2121	17
40	0.71120	2.9289	2.7178	2.4802	0.2375	0.2111	17
41	0.74510	2.9215	2.7113	2.4725	0.2388	0.2102	16
42	0.81268	2.9604	2.7483	2.5146	0.2337	0.2121	15
43	0.82969	2.9867	2.7713	2.5380	0.2333	0.2154	15
44	0.86094	3.0367	2.8154	2.5848	0.2306	0.2213	15
45	0.87893	3.0789	2.8529	2.6233	0.2297	0.2259	15
46	0.89323	3.1152	2.8935	2.6597	0.2339	0.2217	15
47	0.90116	3.1441	2.9219	2.6919	0.2300	0.2221	15
48	0.91586	3.2120	2.9863	2.7586	0.2277	0.2257	14
49	0.92572	3.2651	3.0397	2.8049	0.2348	0.2254	14
50	0.93694	3.3446	3.1095	2.8726	0.2369	0.2351	14
51	0.94761	3.4227	3.1902	2.9551	0.2351	0.2325	18
52	0.95701	3.5022	3.2680	3.0293	0.2388	0.2341	20
53	0.96411	3.5658	3.3291	3.0921	0.2370	0.2367	19
54	0.97286	3.6559	3.4122	3.1683	0.2438	0.2438	19
55	0.98059	3.7199	3.4728	3.2271	0.2457	0.2471	14
56	0.98632	3.7464	3.4929	3.2491	0.2439	0.2534	14
57	0.99215	3.7547	3.5032	3.2539	0.2493	0.2515	14
58	0.99928	3.7596	3.5004	3.2540	0.2464	0.2593	15

[a] orbital phase according to hel. JD $2448687.8026 + 1^{\mathrm{d}}.4950996 \cdot \mathrm{E}$.

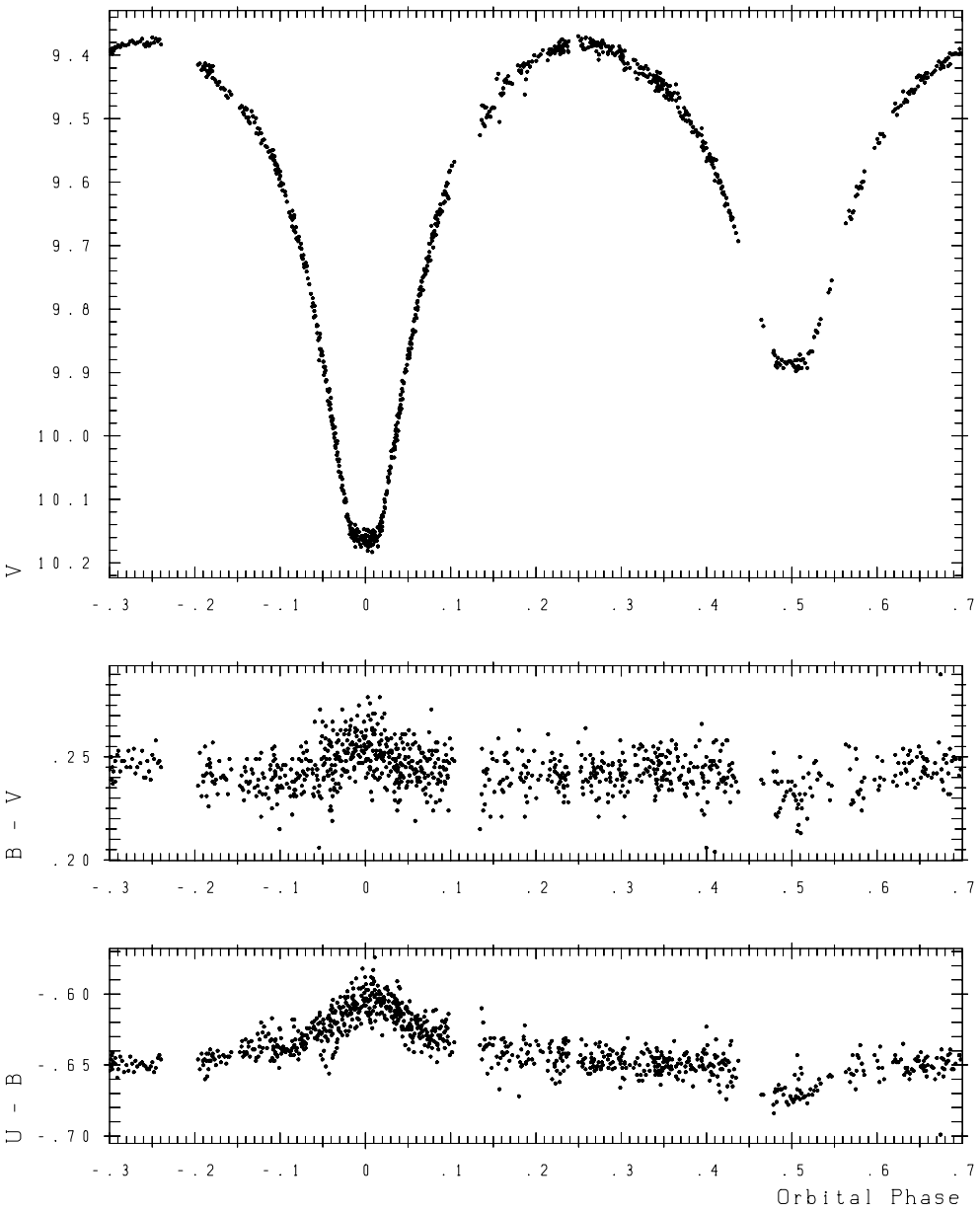

Fig. 5. The observed light curve of the eclipsing binary V606 Cen

(corresponding to B0–0.5 V (cf. Harmanec 1988)), yielding the "H" solution (H for "hot").

In both cases, the bolometric albedos A_1, A_2 and the gravity darkening exponents g_1, g_2 were assumed to be 1.0 as expected for radiative stellar envelopes. The linear limb darkening exponents x_1, x_2 were first fixed at their theoretical values according to calculations by Wade & Rucinski (1985) based on Kurucz model atmospheres, assuming $\log g = 2.84$ corresponding to the spectral classification given above (solution C), and $\log g = 4.00$ for main sequence stars (solution H). In a few cases of the "C" analysis, they were adjusted as well. As the fit quality of convergent "H" solutions with the limb darkening coefficients being fixed at their theoretical values turned out to be not completely satisfying, in the "H" program runs these parameters were generally adjusted. Though there were no hints for the existence of a third body (e.g. as in the cases of IU Aur (Drechsel et al. 1994b) or SZ Cam (Lorenz et al. 1998)), the third light parameters were always adjusted, too. However, in all convergent solutions the third light contribution was not significant, i.e. smaller than about 2 % in all colours.

The UBV light curves were simultaneously solved, using several DEC AXP ALPHA workstations operating with OpenVMS 6.2. After the first trial runs it was already evident that V606 Cen was a contact binary. As due to the complicated potential structure close to the inner Lagrangian point, the MORO code so far does not allow for radiation pressure effects in contact or over-contact systems, the conventional mode, based on the "classical" Roche geometry was applied, and the radiation pressure parameters δ_1, δ_2 were set to zero. Due to our experience, this restriction does not much affect the accuracy of the light curve solution at effective temperatures below, say, 25000 K, where radiation pressure effects are not of great influ-

Table 7. Radiation pressure parameters δ and effective temperatures of the early-type close binaries AB Cru (Lorenz et al., 1994), IU Aur (Drechsel et al., 1994b), SZ Cam (Lorenz et al., 1998), V1331 Aql (Lorenz et al., 1999) and PZ Pup (Kohoutek & Lorenz, 1999), ordered by effective temperatures of the binary components. The system configurations are indicated, too.

Star[a]	$T_{\rm eff}$ (K)	δ[b]	conf.[c]
AB Cru (1)	35800	0.038	d
SZ Cam (1)	33000	0.026	d
IU Aur (1)	32000	0.010	d
IU Aur (2)	28100	0.002	c
SZ Cam (2)	27500	0.018	d
AB Cru (2)	27200	0.015	c
V1331 Aql (1)	25400	0.007	d
V1331 Aql (2)	20100	0.007	dc
PZ Pup (1)	20000	0.004	d
PZ Pup (2)	19500	0.003	d

[a] "1" denotes primary, "2" secondary component of the binary
[b] radiation pressure parameter, defined as ratio of radiative relative to gravitational forces.
[c] Roche configuration of a star: d – detached component, c – component fills critical Roche lobe, dc – component close to critical Roche lobe

ence on the shapes of the light curves of close binaries, as the examples V1331 Aql and PZ Pup show (see Table 7). Therefore, neglecting radiation pressure effects should be acceptable for solution C, wheras the situation is different in case of solution H. Here, δ_1 could be expected to be roughly 1%, when considering stars with effective temperatures in the range from about 27000 K to 32000 K (see Table 7). Lower values are possible, too, as the IU Aur secondary ($T_{\rm eff} = 28100$ K shows. Moreover, in (over-) contact systems such as V606 Cen, the regions of the stellar surfaces of both components, which directly face each other, and hence are mostly exerted to the mutual radiation pressure, are shadowed by the "bottle-neck" connecting both stars. Altogether, using the conventional Roche-model for the light curve analysis of V606 Cen should be an acceptable approximation in the "H" case, too. Additionally, it should be stressed that no detached or semi-detached solutions with reasonable fit quality could be achieved, not even when the radiation pressure option of the MORO program was applied.

The set of adjusted parameters comprised the orbital inclination i, the effective temperature T_2 of the secondary component, the (classical) Roche potentials Ω_1, Ω_2 of the surfaces of both stars, the (photometric) mass ratio $q_{\rm phot}$ (which was always initially given the spectroscopic value 0.527), and the colour dependent quantities L_1 and l_3, representing the luminosity of the primary and the third light contribution, and the linear limb darkening exponents x_1, x_2 in the cases mentioned above.

We achieved a set of 10 convergent "C" solutions with comparable good fit quality (the standard deviation in units of normalized light being about 0.0033, 0.0035 and 0.0026, for U, B and V, respectively). All solutions yielded system configurations close to the marginal contact of both stars.

Table 8. The light curve solutions of V606 Cen. The second column refers to the solution with "cool", the third column refers to the solution with "hot" stellar effective temperatures. To underline that the "H" solution has finally been adopted, the corresponding column is printed in bold characters. For details see text.

parameters	**solution C**	**solution H**
fixed:		
T_1	19 650 K	**29 200 K**
A_1, A_2[a]	1.0	**1.0**
g_1, g_2[b]	1.0	**1.0**
δ_1, δ_2[c]	0.0	**0.0**
adjusted:		
i	$86\overset{\circ}{.}9$ ($\pm 0\overset{\circ}{.}4$)	$\mathbf{87\overset{\circ}{.}3}$ ($\pm\mathbf{0\overset{\circ}{.}1}$)
T_2	15 400 K ($\pm$50 K)	**21 770**K($\pm$**20**K)
$\Omega_1 = \Omega_2$	2.946[d] ($\pm$0.008)	**2.942**[e] ($\pm$**0.002**)
$q_{\rm phot}$	0.540 $\pm$0.006	$\mathbf{0.541 \pm 0.001}$
L_1(U)[f]	0.776 ($\pm$0.002)	**0.766** ($\pm$**0.002**)
L_2(U)[f]	0.224 ($\pm$0.002)	**0.234** ($\pm$**0.002**)
l_3(U)[g]	0.1 % ($\pm$0.5)	**0.3** % ($\pm$**0.1**)
L_1(B)[f]	0.758 ($\pm$0.003)	**0.752** ($\pm$**0.001**)
L_2(B)[f]	0.242 ($\pm$0.003)	**0.247** ($\pm$**0.001**)
l_3(B)[g]	1.0 % ($\pm$0.8)	**1.1** % ($\pm$**0.2**)
L_1(V)[f]	0.742 ($\pm$0.002)	**0.740** ($\pm$**0.001**)
L_2(V)[f]	0.257 ($\pm$0.002)	**0.260** ($\pm$**0.001**)
l_3(V)[g]	0.2 % ($\pm$0.6)	**0.2** % ($\pm$**0.1**)
x_1(U)[h]	0.42 ($\pm$0.01) *0.40*	**0.44** ($\pm$**0.01**) *0.29*
x_2(U)[h]	0.47 ($\pm$0.01) *0.41*	**0.52** ($\pm$**0.01**) *0.34*
x_1(B)[h]	0.36 ($\pm$0.01) *0.39*	**0.38** ($\pm$**0.01**) *0.28*
x_2(B)[h]	0.38 ($\pm$0.09) *0.40*	**0.32** ($\pm$**0.08**) *0.33*
x_1(V)[h]	0.35 ($\pm$0.01) *0.34*	**0.33** ($\pm$**0.01**) *0.24*
x_2(V)[h]	0.37 ($\pm$0.03) *0.34*	**0.38** ($\pm$**0.04**) *0.26*
Roche radii:[i]		
r_1(pole)	0.409 ($\pm$0.001)	**0.410** ($\pm$**0.001**)
r_1(point)	0.567 ($-$)	**0.561** ($-$)
r_1(side)	0.434 ($\pm$0.001)	**0.435** ($\pm$**0.001**)
r_1(back)	0.462 ($\pm$0.001)	**0.464** ($\pm$**0.001**)
r_2(pole)	0.307 ($\pm$0.001)	**0.308** ($\pm$**0.001**)
r_2(point)	0.433 ($-$)	**0.439** ($-$)
r_2(side)	0.321 ($\pm$0.001)	**0.322** ($\pm$**0.001**)
r_2(back)	0.354 ($\pm$0.001)	**0.356** ($\pm$**0.001**)

[a] bolometric albedos
[b] gravitational darkening exponents
[c] radiation pressure parameters
[d] corresponding to $f_\Omega = 0.02$ (see text)
[e] corresponding to $f_\Omega = 0.04$ (see text)
[f] relative luminosities $L_i/L_1 + L_2$;
[g] fraction of third light at maximum;
[h] linear limb darkening coefficients; theoretical values taken from Wade & Rucinski(1985) are given in italics
[i] fractional Roche radii in units of separation of mass centers

The level of over-contact can be described as

$$f_\Omega = \frac{\Omega_{iLp} - \Omega}{\Omega_{iLp} - \Omega_{oLp}} \quad , \tag{3}$$

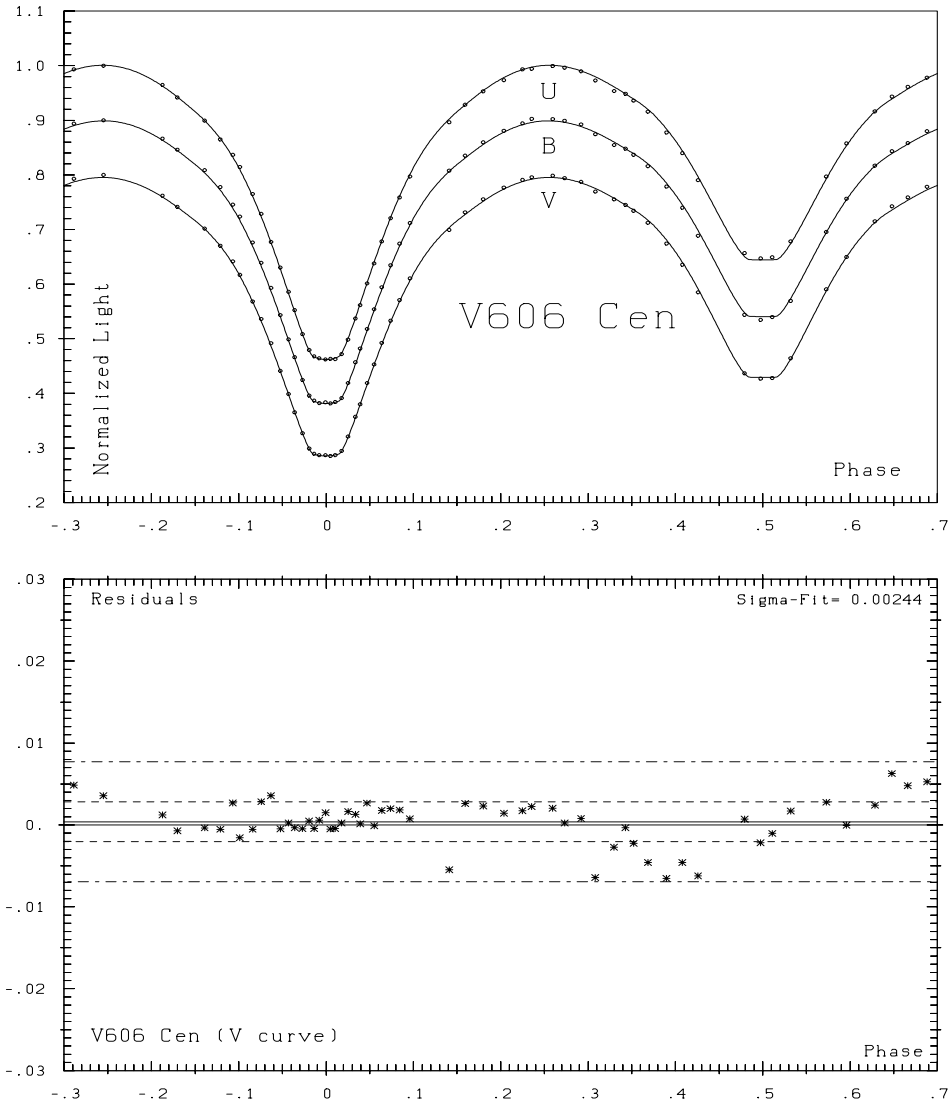

Fig. 6. *Top:* computed UBV curves ("H" solution) of V606 Cen together with normal points from Table 6. *Bottom:* residuals between the V curve and normal points. The mean residual is $-3.8{\cdot}10^{-4}$, weighted standard deviation is $2.44 \cdot 10^{-3}$. 1σ and 3σ belts are shown as dashed and dash-dotted lines, respectively.

with Ω being the (identical) surface potential of both stellar components, and Ω_{iLp} and Ω_{oLp} representing the potential of the inner and outer Lagrangian point, respectively. In all of our light curve soutions, f ranged from 0.01 to 0.04, which is very close to the exact contact configuration ($f_\Omega = 0.00$).

As the definite "C" system solution, we chose the one with the very best fit quality. In this solution the x_1, x_2 parameters were fixed at the values, which had been adjusted in a previous program run, being very close to their theoretical values.

A total of 27 convergent "H" light curve solutions was obtained with fit qualities comparable to the one of the best "C" solution. 7 solutions out of these showed even slightly better standard deviations. The numerical best one was selected as definite "H" solution, with standard deviations of 0.0034, 0.0033, and 0.0024 for the U, B, and V curve, respectively.

The light curve solutions are listed in Table 8. Besides the effective temperatures, the differences between both solutions are marginal. The given errors represent the scatter of the parameter values achieved in the individual light curve solutions with comparable high fit quality. It should be stressed that the obtained values for the photometric mass ratio always lay within the error limits of the spectroscopic one. This fact supports the consistency of our light curve solutions with the spectroscopic results.

A plot of the calculated UBV curves together with the normal points, and, as an example, the residuals of the V curve are presented in Fig. 6. A meridional intersection of the V606 Cen system is shown in Fig. 7, and Fig. 8 presents a 3D simulation of the V606 Cen contact binary, seen at various orbital phases with the realistic inclination angle of $87\overset{\circ}{.}3$ – we call it the "Roche movie" of V606 Cen. All these figures refer to the "H" solution.

4. Discussion

4.1. Absolute dimensions, effective temperatures and equivalent widths

Initially, absolute dimensions of V606 Cen based on the "C" solution (see Table 8) were calculated. For this purpose the photometric mass ratio and the spectroscopic radial velocity ampli-

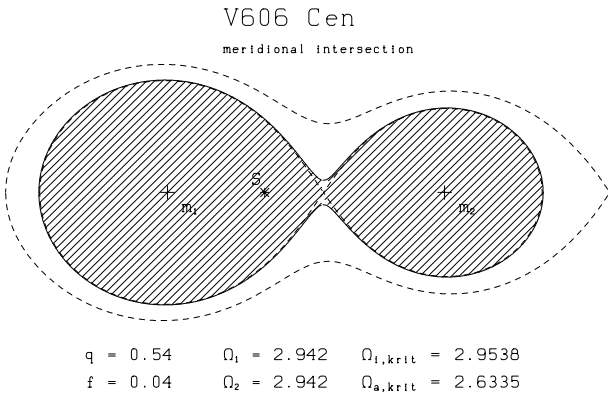

Fig. 7. Meridional intersection of V606 Cen according to the parameters of the light curve solution "H" given in Table 8.

Table 9. Absolute dimensions of V606 Cen according to light curve solutions with low ("solution C") and high ("solution H") effective stellar temperatures. To underline that the "H" solution is considered to be the definite one, the corresponding column is printed in bold characters. For details see text.

	solution "C"	**solution "H"**
$\log\ T_1$	4.29	**4.47**
$\log\ T_2$	4.19	**4.34**
$M_1/\mathrm{M}_\odot$	14.73 ($\pm$0.41)	**14.70** ($\pm$**0.40**)
$M_2/\mathrm{M}_\odot$	7.96 ($\pm$0.24)	**7.96** ($\pm$**0.22**)
$R_1/\mathrm{R}_\odot$ [a]	6.81 ($\pm$0.06)	**6.83** ($\pm$**0.06**)
$R_2/\mathrm{R}_\odot$ [a]	5.13 ($\pm$0.05)	**5.19** ($\pm$**0.05**)
$L_1/\mathrm{L}_\odot$	6.21 ($\pm$0.28) $\cdot 10^3$	**3.04** ($\pm$**0.10**) $\cdot$ **10^4**
$L_2/\mathrm{L}_\odot$	1.33 ($\pm$0.03) $\cdot 10^3$	**5.44** ($\pm$**0.11**) $\cdot$ **10^3**
$\log L_1/\mathrm{L}_\odot$	3.79 ($\pm$0.02)	**4.48** ($\pm$**0.01**)
$\log L_2/\mathrm{L}_\odot$	3.12 ($\pm$0.01)	**3.74** ($\pm$**0.01**)
$\log\ g_1$	3.94 ($\pm$0.01)	**3.94** ($\pm$**0.01**)
$\log\ g_2$	3.92 ($\pm$0.01)	**3.91** ($\pm$**0.01**)

[a] radius of sphere with same surface area as distorted star;

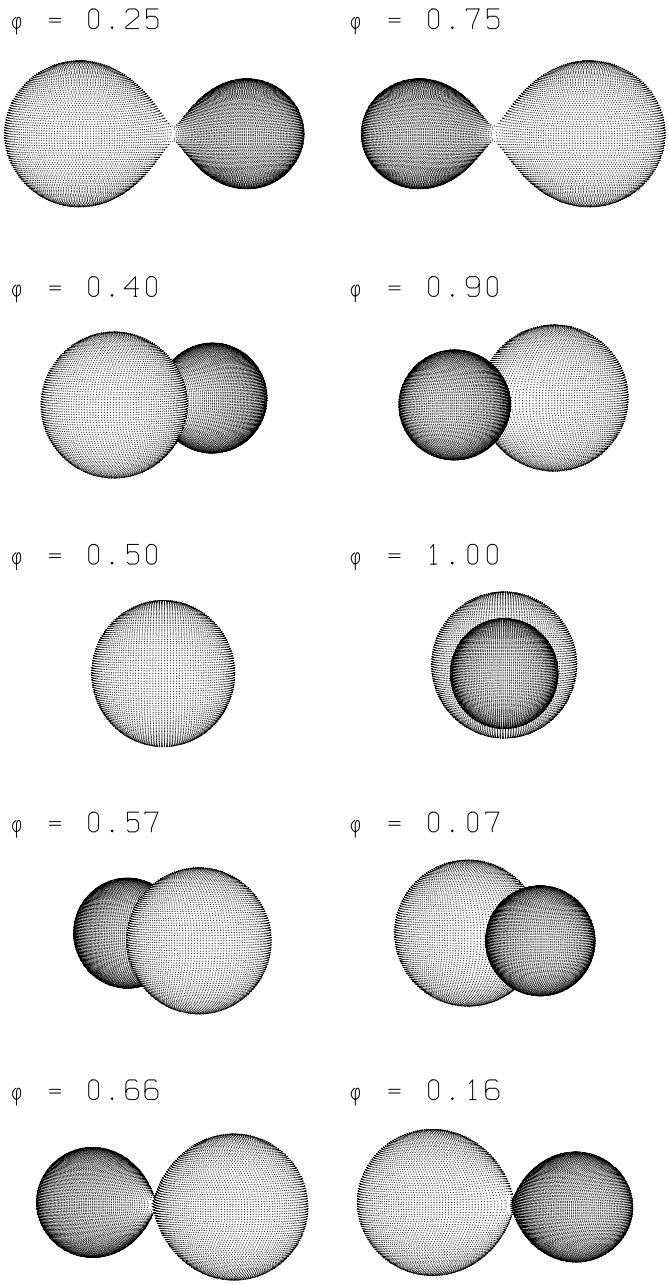

Fig. 8. The V606 Cen "Roche movie": a 3D simulation of the contact system shown at various orbital phases, based on the results of the light curve solution "H" given in Table 8.

tudes K_1 and K_2 were used. The luminosities were calculated with the adopted effective temperature $T_1 = 19650$ K of the primary, the adjusted effective temperature $T_2 = 15400$ K of the secondary, and using the surface areas of the distorted stars, as computed by the MORO program. The resulting absolute stellar parameters of V606 Cen are collected in Table 9.

The masses and radii derived this way were compared with values from a compilation of observed stellar quantities by Harmanec (1988), who gives $M = 16.5\,\mathrm{M}_\odot$, $R = 6.7\,\mathrm{R}_\odot$ corresponding to spectral type B0 V, and $M = 12.2\,\mathrm{M}_\odot$, $R = 6.1\,\mathrm{R}_\odot$ corresponding to spectral type B0.5 V. The actual mass of the V606 Cen primary of $14.7\,\mathrm{M}_\odot$ therefore fits a spectral type between B0 V and B0.5 V, which corresponds to an effective temperature of about 29200 K. The spectral type B0–B0.5 of the primary is also supported by the colour index of this star, which can be determined without contamination by the secondary component, since the secondary minimum is due to a total eclipse (see Sect. 3.1). The determined primary radius of $6.8\,\mathrm{R}_\odot$ is in good agreement with B0 V, too. Considering the secondary, its mass of $8.0\,\mathrm{M}_\odot$ is similar to the one of a B2 V star ($M = 8.6\,\mathrm{M}_\odot$), the measured radius of $5.1\,\mathrm{R}_\odot$, however, is about $1\,\mathrm{R}_\odot$ larger than indicated in Harmanec's (1988) compilation.

On the other hand, a comparison of the derived masses and radii with tables by Schmidt-Kaler (1982) for supergiants, as it would be required due to the spectral classification by Houk & Cowley (1975), does not lead to any satisfying coincidence: for stars with masses similar to those of the V606 Cen primary and

secondary, the predicted radii are by a factor of about 5 and 8, respectively, too large. As a matter of fact, there is no supergiant or even giant radius table value, which is in agreement or only close to our measured radii of V606 Cen. This fact as well as the observed surface gravities (see Table 9), which are considerably larger than expected for giants or supergiants, must be considered as a strong argument in favour of a main sequence nature of both stars.

Altogether, another light curve analysis with higher effective temperatures (corresponding to spectral types B0–0.5 V and B2 V for the primary and secondary, respectively) was required. Consequently, the light curves of V606 Cen were re-analyzed with a fixed primary temperature $T_1 = 29200$ K as described in Sect. 3.2 ("H" solution). The adjusted secondary effective temperature was $T_2 = 21770$ K, consistent with a spectral type B2–3 V (Harmanec 1988). The derived masses, radii and $\log g$ are nearly equal to the values obtained for the lower effective temperatures, whereas, of course, the luminosities are quite different (see Table 9). The fit quality of the "H" solution is practically identical with the one of the "C" solution.

Generally, effective temperatures can be checked by the comparison of measured equivalent widths of the spectral lines with modern calculations based on stellar atmosphere models. Hence, the (true) EWs of He I 4922 as given in Table 3, "C" solution, were compared with LTE-calculations by Lemke (1998), based on ATLAS9 Kurucz model atmospheres, using the LINFOR code (originally developed at Kiel University by Holweger, Steffen & Steenbock and modified by Lemke), and line broadening tables by Barnard et al. (1974) and Shamey (1969). As NLTE effects are of increasing importance at effective temperatures above 25000 K, the primary EWs of the "H"solution were compared with NLTE-grids by Napiwotzki (1998), which are briefly described by Lorenz et al. (1998).

Unfortunately, as discussed in Sect. 2.3, the EWs of V606 Cen show a strong dependence on orbital phase, which makes the comparison with calculated quantities problematic. The only practicable way was to use the overall mean of the true EWs for this purpose. The average true and the calculated EWs of He I 4922 are collected in Table 10. Note that the average EWs of the "C" solution differ only by 0.001 Å from the ones based on the "H" solution.

Considering the upper part of Table 10, which corresponds to the "C" solution, it is evident that the measured EW of the primary fairly fits the calculated one, whereas the measured secondary EW exceeds the theoretical value by nearly 60%, but still lying within the error limit. On this point, a slightly higher effective temperature or a certain helium over-abundance of the secondary might be assumed.

The situation is different or strictly-spoken inverse in the case of the "H" solution. Here, the measured primary EW is about 25% larger than predicted by the NLTE calculations, but still within the error limits, too, whereas the one of the secondary is nearly equal to the LTE table value. Here, a certain amount of helium over-abundance in the primary's atmosphere could be present. Because of the error limits of the true EWs, which are rather large due to their phase dependence, the examination of the He I 4922 equivalent widths does unfortunately not lead to a clear decision in favour of or against one of the given light curve solutions.

Table 10. Comparison between measured (true) and calculated equivalent widths of He I 4922. Solar abundances and $\log g = 4.0$ are assumed. Values referring to effective temperatures according to the C and H solution are printed in bold characters.

$T_{\rm eff}$ in K	true EW in Å	calc. EW in Å	model[a]
	C solution		
22000	–	0.73	LTE
20000	–	0.77	LTE
19650	**0.82±0.15**	**0.76**	LTE
18000	–	0.72	LTE
15400	**0.77±0.32**	**0.49**	LTE
15000	–	0.45	LTE
	H solution		
30000	–	0.64	NLTE
29200	**0.82±0.15**	**0.66**	NLTE
27000	–	0.71	NLTE
24000	–	0.65	LTE
21770	**0.77±0.32**	**0.73**	LTE
20000	–	0.77	LTE

[a] for details see text

Generally, a useful temperature indicator for stars with spectral type around B0 is the strength of He II. As shown by Grigsby et al. (1992), who gave a collection of measured EWs of He II 4686, this line becomes detectable at effective temperatures above about 25000 K. Therefore, it seemed reasonable to look for He II 4686 lines in our ECHELEC spectra, which comprised the corresponding spectral range. As a matter of fact, no presence of this line at all was detected in any spectrum. However, since the ECHELEC spectra have only moderate S/N ratios (about 30), it could not be excluded that weak line features of He II 4686 were masked by considerable noise. In order to estimate the required strength of a line to be even detectable, synthetic spectra with noise similar to that of the ECHELEC spectra and single Gaussian profiles of different (known) equivalent widths were created and tested with respect to the visibility of this profiles. The FWHMs of the Gaussians were chosen to be comparable to those of the measured He I 4922 lines of the primary component. It turned out that profiles with an (observed) EW of 0.25 Å, corresponding to a (phase-dependent) true EW of about 0.35 Å, were marginally detectable. Hence, this value represents a lower limit for the visibility of He II 4686 lines in our ECHELEC spectra, and it was therefore compared with the observed correlation between the He II 4686 line strength and the effective temperature (see Grigsby et al. 1992). We found $T_{\rm eff} \approx 29000$ K corresponding to EW ≈ 0.35, which is only an approximation, due to the scattering of the data published by these authors.

Unfortunately, this effective temperature is almost exactly the one, which we adopted for the V606 Cen primary in the

"H" case. For that reason, the non-visibility of He II 4686 in the ECHELEC spectra only indicates that the V606 Cen primary might not be much hotter than 29000 K. But on the other hand, from this point of view it might certainly also be as "cool" (19650 K) as assumed for the "C" solution.

The expected EW of He II 4686 according to the NLTE calculations by Napiwotzki (1998) for a star with $T_{\rm eff} = 29200$ K and $\log\ g = 4.0$ is 0.12 Å, and therefore clearly below the mentioned limit of about 0.35 Å.

After all, there are no important objections against the H solution, but strong arguments in favour of it. One should not forget that spectral classifications based on objective prism spectroscopy generally are not very reliable in case of close binaries, because of the existence of double lines or line blends, which possibly have not been taken into account. The supergiant spectral type of V606 Cen given by Houk & Cowley (1975) might be a consequence of this, and should therefore not be given too much weight. The masses, radii, and, in particular, the surface gravities of both stellar components, which are typical for main-sequence stars, let us suggest spectral types B0–0.5 V and B2–3 V for the primary and secondary of V606 Cen, respectively, and therefore we consider the H light curve solution as the definite one.

4.2. Evolutionary state and comparison with other close contact binaries

The stellar components of V606 Cen were compared with other interacting binaries listed by Harries & Hilditch (1998). In Fig. 3 of their paper, which gives a mass-log-g diagram with evolutionary tracks for single stars by Schaller et al. (1992), the secondaries of semi-detached systems appear as evolved and over-luminous stars, as it is expected when they fill their Roche lobes. The primary of V606 Cen is located close to an isochrone representing an age of 6 Myr, whereas the secondary lies clearly beyond the 7 Myr isochrone. With respect to their masses and surface gravities (and additionally to the orbital period P≈$1\overset{\rm d}{.}8$) both components of V606 Cen are similar to those of IU Aur, which however is a semi-detached binary. The surface gravity of the V606 Cen secondary ($\log\ g = 3.91$) is higher than the one of any other secondary of similar mass listed by these authors (XZ Cep: $\log\ g = 3.20$, AB Cru: $\log\ g = 3.39$, LZ Cep: $\log\ g = 3.48$, and IU Aur: $\log\ g = 3.79$), which underlines the main sequence nature of this star.

Since the inclusion of convective core-overshooting and stellar wind mass loss in evolutionary concepts for close binaries (cf. e.g. Sybesma 1985 and 1986) it has been clear that contact configurations are possible already during the main-sequence state. Sybesma (1985) noted that systems with initial masses of 20+10 $\rm M_\odot$ ($q_{\rm i} = 0.5$) and initial orbital periods shorter than about 3 d evolve into a short-lived contact configuration during the rapid phase of case A mass transfer (case A(r)), whereas binaries with higher initial mass ratios ($q = 0.8$, $q = 0.9$) and still smaller periods form more stable contact systems close to the end of case A mass transfer, i.e. within its slow phase (case A(s); Sybesma 1986). The well-known compilation by Hilditch & Bell (1987), which comprises 7 contact systems and compares observational data with stellar evolutionary grids, confirms that these binaries appear to be in contact states achieved after case A(r) and during case A(s) mass transfer phases.

As it is evident that both components of V606 Cen are still on the main sequence, case A mass transfer should be responsible for the contact nature of this system, too. Comparing the masses, radii and luminosities of V606 Cen with results of a more recent compilation by Figueiredo et al. (1994), who expand the data base of Hilditch & Bell (1987) by some more early-type close binaries, it is clear that the V606 Cen components align very well with the row of the stars studied there. In their mass-luminosity diagram, the primary as well as the secondary would be placed nearly exactly on the line which represents the core hydrogen contents $X_{\rm c} = 0.35$, having been calculated by means of single star models. Note that the luminosities of the V606 Cen components as derived from the "C" solution ($\log L_1/{\rm L}_\odot = 3.79$; $\log L_2/{\rm L}_\odot = 3.12$) would be considerably lower than the ZAMS luminosities ($\log L_1/{\rm L}_\odot({\rm ZAMS}) \approx\ 4.3$; $\log L_2/{\rm L}_\odot({\rm ZAMS}) \approx\ 3.4$) for the determined masses (which are nearly equal for solution "C" and "H"; see Table 9). In the mass-radius diagram of the paper by Figueiredo et al. (1994) the secondary hits the $X_{\rm c} = 0.35$ line, too, whereas the primary is located at about $X_{\rm c} = 0.45$, i.e. slightly closer to ZAMS.

Figueiredo et al. (1994) also claim that case A(s) mass transfer should be the cause for the contact configuration of the binaries treated in their paper. With respect to its evolutionary state, V606 Cen is therefore comparable to systems like V382 Cyg (Harries et al. 1997), V701 Sco (Bell & Malcolm 1987a) and RZ Pyx (Bell & Malcolm 1987b), whereas V348 Car (Hilditch & Lloyd Evans 1985), LY Aur (Drechsel et al. 1989) and AO Cas (Gies & Wiggs 1991) represent a slightly more evolved state.

These results are supported by a comparison of the observed quantities of V606 Cen with evolutionary grids by Pols (1994), especially treating the case A mass transfer phases, however not taking overshooting and stellar wind mass loss into consideration. One calculated model system, which is comparable to the observed properties of V606 Cen, consists of a primary with $M_{\rm I} = 16\,{\rm M}_\odot$ and a secondary with $M_{\rm II} = 12\,{\rm M}_\odot$, representing the initial masses, and with a start period $P_{\rm i} = 1\overset{\rm d}{.}5$. The initial core hydrogen contents amount to $X_{\rm c,I} = 0.44$ and $X_{\rm c,II} = 0.55$. This system approaches marginal contact during the short case A(r) mass transfer phase after $5.7 \cdot 10^6$ yr, which only lasts about $5 \cdot 10^4$ yr. After that, the orbital period has increased to $1\overset{\rm d}{.}65$, and the secondary (II) is the more massive star ($M_{\rm I} = 10.8\,{\rm M}_\odot$; $M_{\rm II} = 17.2\,{\rm M}_\odot$), i.e. inversion of the mass ratio has taken place. Its core hydrogen contents have grown ($X_{\rm c,II} = 0.62$) due to the fact that "fresh" hydrogen is mixed into the stellar centre. After an "Algol-like" semi-detached phase, when the secondary continues accreting mass from the primary (case A(s) mass transfer), it will expand to the critical Roche-lobe itself, then forming a contact binary. This will occur close to the end of case A(s) mass transfer (which lasts about $6.7 \cdot 10^6$ yr) at an age of $12.9 \cdot 10^6$ yr. Then the masses are $M_{\rm I} = 7.3\,{\rm M}_\odot$ and $M_{\rm II} = 20.7\,{\rm M}_\odot$, the period now being

$3\overset{\mathrm{d}}{.}07$, and $X_{\mathrm{c,I}} = 0.12$ and $X_{\mathrm{c,II}} = 0.10$. Though the actual masses of the V606 Cen components are different from those of the model system, its evolution should be comparable to the one of V606 Cen. Pols underlines that the shorter the initial period was, the earlier a contact binary is formed. As the actual orbital period of V606 Cen is $1\overset{\mathrm{d}}{.}5$, a shorter initial period (and, of course, slightly different start masses) than given for this model system could be assumed. This would result in a contact configuration already in an earlier stage of the case A(s) phase, moreover probably yielding slightly higher core hydrogen contents, close to those found for V606 Cen, when using the Figueiredo (1994) compilation.

This is supported when looking at the evolutionary track of a 8+7 $\mathrm{M}_\odot$ system with $P_{\mathrm{i}} = 0\overset{\mathrm{d}}{.}98$, also given in the Pols (1994) paper. This system evolves into a contact configuration during case A(s) mass transfer with $M_{\mathrm{I}} = 5.7\,\mathrm{M}_\odot$, $M_{\mathrm{II}} = 9.4\,\mathrm{M}_\odot$ and $P = 1\overset{\mathrm{d}}{.}17$ after $21.3 \cdot 10^6$ yr, with the case A(s) phase lasting about 10^7 yr.

Though in both cases discussed above neither the masses nor the orbital periods exactly fit the observed quantities of V606 Cen, it seems that V606 Cen has probably evolved into a contact system during the slow phase of case A mass transfer, with its stellar components still being placed on the broadened main-sequence. As Pols notes, such contact binaries, formed in a stable manner, and with both stars being in thermal equilibrium, are stable themselves. Hence we consider V606 Cen as another member of the group of early-type contact binaries with main-sequence stellar components listed by Hilditch & Bell (1987) and Figueiredo et al. (1994).

5. Conclusions

With V606 Cen it was possible to add one more member to the very limited sample of early-type contact binaries (Figueiredo et al. 1994 indicate 11 systems, though only 7, which had already been discussed in the paper by Hilditch & Bell (1987), are explicitely presented including their stellar characteristics), for which accurate stellar parameters are known. The components of this system are located well within the main-sequence band, and the contact configuration was very likely formed during the slow phase of case A mass transfer. For a better comparison of observed quantities with the evolution theory for close binaries, "denser" evolutionary grids, in particular for short period systems would be desirable.

As it was shown in this paper, the determination of accurate effective temperatures of the stellar components is crucial for the exact study of such systems. Spectral classifications based on objective prism spectra are probably not well suited for the derivation of effective temperatures, especially in the case of close binaries. Normally, the comparison of observed and calculated equivalent widths might help to solve this problem, unless variable EWs make it impossible. Therefore, the development of other tools to fix effective temperatures better would be very desirable. The strong variability of the He I lines in the spectra of V606 Cen with the orbital phase, i.e. the so far unexplained "Struve-Sahade effect", is certainly another important field for further investigations.

Acknowledgements. We like to thank Drs. M. Lemke and R. Napiwotzki (Dr.-Remeis-Sternwarte, Bamberg) for kindly carrying out model atmosphere calculations for the determination of equivalent widths. This work was supported in part by the *Deutsche Forschungsgemeinschaft, DFG* grants Dr 131/8-2,3 and 436 CSR 113/39/1. The assistance of the staff of the *European Southern Observatory* at La Silla, Chile, is gratefully acknowledged.

References

Barnard A.J., Cooper J., Smith E.W., 1974, JQSRT 14, 1025
Bell S.A., Malcolm G.J., 1987a, MNRAS 226, 899
Bell S.A., Malcolm G.J., 1987b, MNRAS 227, 481
Drechsel H., Lorenz R., Mayer P., 1989, A&A 221, 49
Drechsel H., Haas S., Lorenz R., Gayler S., 1994a, A&A 294, 723
Drechsel H., Haas S., Lorenz R., Mayer P., 1994b, A&A 284, 853
Drechsel H., Weeber M., Lorenz R., Hadrava P., 1997, Astron. Ges. Abstr. Ser. 13, 207
Eggen O.J., 1978, ApJ 83(3), 288
Figueiredo J., De Greve J.P., Hilditch R.W., 1994, A&A 283, 144
Gies D.R., Wiggs M.S., 1991, ApJ 375, 321
Gies D.R., Bagnuolo jr. W.G., Penny L.R., 1997, ApJ 479, 408
Grigsby J.A., Morrison N.D., Anderson L.S., 1992, ApJS 78, 205
Hadrava P., 1995, A&AS 114, 393
Harmanec P., 1988, BAC 39, 329
Harries T.J., Hilditch R.W., 1998, Boulder-Munich II: Properties of Hot, Luminous Stars. ASP Conference Series, Vol. 131, 401
Harries T.J., Hilditch R.W., Hill G., 1997, MNRAS 277, 287
Hertzsprung E., 1950, Ann. Leiden 20, 119
Hilditch R.W., Lloyd Evans T., 1985, MNRAS 213, 75
Hilditch R.W., Bell S.A., 1987, MNRAS 229, 529
Houk N., Cowley A., 1975, Univ. of Michigan Cat. of two- dimensional spectral types for the HD stars. Ann Arbor, Michigan
Kohoutek L., Lorenz R., 1999, A&A, in preparation
Lemke M., 1998, priv. comm.
Lorenz R., Mayer P., Drechsel H., 1994, A&A 291, 185
Lorenz R., Mayer P., Drechsel H., 1998, A&A 332, 909
Lorenz R., Drechsel H., Mayer P., 1999, A&A, in preparation
Mayer P., Hadrava P., Harmanec P., Chochol D., 1991, BAC 42, 230
Mayer P., Drechsel H., Lorenz R., 1992, IBVS 3805
Mayer P., Lorenz R., Drechsel H., 1999, A&A, in preparation
Napiwotzki, R., 1998, priv. comm.
Pols O.R., 1994, A&A 290, 119
Schaller G., Schaerer D., Meynet G., Maeder A., 1992, A&AS 96, 296
Schmidt-Kaler Th. 1982, In: Landolt-Börnstein Vol. 2b, Springer-Verlag Berlin, Heidelberg, New York, p. 31
Shamey L.J., 1969, Ph.D. Thesis, B.S. Loyola University of Los Angeles
Stephenson C.B., Sanduleak N., 1971, Publ. Warner and Swasey Obs. 1, 1
Stickland D.J., 1997, The Observatory 117, 37
Stickland D.J., Lloyd C., Koch R.H., Pachoulakis I., 1995, The Observatory 115, 317
Struve O., 1950, Stellar Evolution. Princeton University Press, p. 182
Swope H., 1939, Harvard Annals 90, 178
Sybesma C.H.B., 1985, A&A 142, 171
Sybesma C.H.B., 1986, A&A 159, 108
Wade R.A., Rucinski S.M., 1985, A&AS 60, 471